Eur. Phys. J. D **18**, 51–59 (2002)
DOI: 10.1140/e10053-002-0006-7

THE EUROPEAN PHYSICAL JOURNAL D
EDP Sciences

Study of the far wing of the Balmer α line of hydrogen perturbed by collisions with protons

Balmer α

J.F. Kielkopf[1,a], N.F. Allard[2,3], and A. Decrette[4]

[1] Department of Physics, University of Louisville, Louisville, Ky 40292, USA
[2] Observatoire de Paris-Meudon, Département Atomes et Molécules en Astrophysique, 92195 Meudon Principal Cedex, France
[3] CNRS Institut d'Astrophysique, 98 bis Boulevard Arago, 75014 Paris, France
[4] Laboratoire de Recherche sur la Réactivité des Solides, Université de Bourgogne[b], 9 avenue Alain Savary, B.P. 47870, 21078 Dijon Principal Cedex, France

Received 11 October 2001

Abstract. The theory of the Balmer α line of atomic hydrogen perturbed by collisions with protons predicts quasi-molecular satellites in the line wing due to H–H^+ collisions. Measurements of the spectrum of a laser-produced plasma confirm the existence of the strongest of these features.

PACS. 32.70.Jz Line shapes, widths, and shifts – 95.30.Dr Atomic processes and interactions – 95.30.Ky Atomic and molecular data, spectra, and spectral parameters (opacities, rotation constants, line identification, oscillator strengths, gf values, transition probabilities, etc.) – 97.20.Rp Faint blue stars (including blue stragglers), white dwarfs, degenerate stars, nuclei of planetary nebulae

1 Introduction

Recently we have found that the conditions in a laser-produced hydrogen plasma in the laboratory are similar to those in white dwarf stellar atmospheres [1–7]. A theoretical model of this source based on heating by the propagation of a shock wave demonstrates that the molecular hydrogen is totally dissociated, leaving partially ionized atomic hydrogen in the region from which its optical, ultraviolet, and vacuum ultraviolet spectrum originates. This permits repetitive well-diagnosed experiments in support of spectral line shape theory and astronomical observation, and study of atomic processes in hydrogen at densities of neutral atoms, ions, and electrons an order of magnitude larger than in previous work with arcs and pinch discharges. Consequently, new experimental data test theories of spectral line formation that include radiative processes during the atom-atom and atom-ion collisions that are probable in dense plasmas. Previous work on the Lyman series [2,8,3–7] was used to explain the far ultraviolet spectra of hydrogen-rich white dwarfs [9–12] and Lambda Boo stars [13]. The continuation described here is concerned with the Balmer series.

Although methods of calculating the complete spectral line profiles have been known for some time, only recently have comprehensive calculations of the Lyman α and Lyman β line wing been made that include perturbations by both neutrals and ions in all possible quasi-molecular states of H_2 and H_2^+ [7]. Structures in the Lyman α and Lyman β line wing have been identified with free-free transitions which take place during binary close collisions of the radiating H atom and a perturbing atom or ion [4–6]. We have now explored the Balmer α wing to determine whether such features could appear in this wavelength domain.

New calculations of the total profile of the atomic hydrogen Balmer α spectral line perturbed by collisions with protons were made using the theory of spectral line broadening described in detail by Allard *et al.* [6]. Our approach requires prior knowledge of accurate theoretical molecular potentials to describe the interaction between radiator and perturber, and knowledge of the variation of the radiative dipole moment with atom-ion separation for each molecular state. Although accurate H_2^+ potentials have been tabulated by Madsen and Peek [14], and H_2^+ dipole transition moments have been calculated by Ramaker and Peek [15], comprehensive self-consistent neutral molecular data, including radiative transition moments and electron-atom interactions, required for modeling the effect of atom-atom

[a] e-mail: john@nimbus.physics.louisville.edu
[b] UMR 5613 du CNRS

and atom-electron collisions on the spectrum, were not yet available. For this reason, we focus our interest here on collisions with protons and neglect the neutral and electronic contributions which are nevertheless both very important. Even with this restriction, the computation of the complete profile perturbed by protons requires taking into account in detail the large number of states which contribute to the Balmer line. Through difference potential extrema, variation of the electronic transition moment with atom-ion distance, and the effect of the Boltzmann factor, each of these states may lead to structure in the far line wing.

Although the broadening of the core of the Balmer α line is now fairly well understood, at least at low density [16], the spectrum far from the line center is complex, and has been largely unknown. We will describe the experiments, and compare the observed spectra to unified theoretical Balmer α profile calculations.

2 Laboratory spectra

The underlying premise of the experimental work is that laser energy deposited on nanosecond timescales in a pure H_2 gas target results in shock heating, excitation, dissociation and ionization of the molecular gas. The hot plasma which results provides an object for studies of the spectrum of atomic H under high density and at high temperature. Given spatial and temporal resolution of the shock and its aftermath, spectroscopy over a wide range of densities is possible, up to at least the initial static gas fill density in the target cell. The conditions found in this plasma are not accessible to the more conventional laboratory experiments which have been used for previous line profile studies of the Balmer series. When the target is pure H_2 at atmospheric pressure, the shockfront for a plasma produced by focusing a 6 ns, 600 mJ, 1064 nm pulse of Nd:YAG laser light initially moves at over 10 times the sound speed in the gas. As it moves outward, the shock compresses and heats the molecular gas, dissociates it into atomic H, and produces a fully ionized plasma behind the front. By 2 μs after the initiating laser pulse, the shock is 6 mm from the optical axis and slowed to less than twice speed of sound. It surrounds the bubble of hot recombined atomic H it produced, which follows it as an outward flow of hot gas from the interior. The conditions behind the front are a consequence of the steep temperature gradient which results from the sudden release of energy near the axis. This leads to a spatially defined shell in which the gas is hot enough to emit the Balmer series, but not so hot that it is fully ionized. The hydrodynamic and optical properties of the plasma and the resulting post-plasma bubble have been described elsewhere [1,3,17].

Definitive studies of the Hα and Hβ lines of the Balmer series have been reported for a well-diagnosed wall-stabilized arc up to a density of 10^{17} cm^{-3} [18], and for a gas-liner pinch up to a density of 10^{19} cm^{-3} [19]. While those experiments were directed at determining the shape and width of the line within a few halfwidths of the line center, there have been no indications that the profiles are structured in the way in which the theory we will describe here predicts. To the contrary, the profiles match theories in which the dominant broadening mechanism is electron collisions, and in which the ion and neutral collisions we emphasize here were treated only approximately or not at all. Indeed, preliminary experiments in our laboratory showed Balmer series line cores in agreement with standard Stark profile theory, as expected. Nevertheless, we have seen effects on Lyman α in the so-called far wing, that is, in regions out 20 000 or more cm^{-1} on the low-energy side of the line center, partly by taking advantage of the self-reversal of the line core in emission which reduces stray light in the far wing. In the case of the Balmer series, of course, such extreme perturbations cannot be seen since generally the line does not reverse, and since Hα is at 15 237 cm^{-1} and interesting regions associated with strong collisions of the $n = 3$ states lie in the infrared or overlap other members of the series. There are, however, two regimes that are accessible experimentally, and have not previously been explored: the red wing of Balmer α out to 1 μm, and the line shape when ion or neutral densities exceed 10^{19} cm^{-3}.

The experimental arrangement is illustrated in Figure 1. A pulsed Nd:YAG laser produces 1.064 μm light which is steered down the axis of a high pressure gas cell. The experiments described here used pulse energies of 300 to 600 mJ, although the data shown are all for energies of 300 mJ. At a pulse duration of about 6 ns, the average power per pulse was nominally 50 MW. This light was imaged into the cell by a fused silica, 10 cm focal length, plano-convex lens in a minimum spherical aberration configuration, producing a spot size of the order of 20 μm and an energy flux of 1.6×10^{13} W cm^{-2}. At the pressures used in this experiment, self-focusing of the laser by the plasma caused the effective focal point to move toward the lens several millimeters, and led to the formation of a channel with a diameter of the order of the focal spot size.

The gas cell was a thick-wall aluminum cylinder 5 cm in diameter and 10 cm long, bored to 2 cm inside diameter along its axis. The observation port was on a radius of the cylinder such that it looked into the gas manifold port. This provided a black background to minimize detection of light scattered from other parts of the cell. Windows were attached with stainless steel fittings and O-ring seals. The entrance and exit windows for the laser were 3 mm thick fused silica 2.5 cm in diameter. The observation window was either fused silica or MgF_2, 1 cm in diameter and 2 mm thick. These windows were sufficiently strong to withstand H_2 pressures up to 100 atm (10^7 pascal) under static load without failure. We caution, however, that one failure attributed to a mounting stress fracture of the MgF_2 observation window occurred. In general a window failure which results in a crack should not be catastrophic, since the H_2 release would be slow. However, this cell stores a total energy of 10 joules in the compressed gas which could cause damage or injury in sudden failure. It was this concern that set the limit of 100 atm for these experiments.

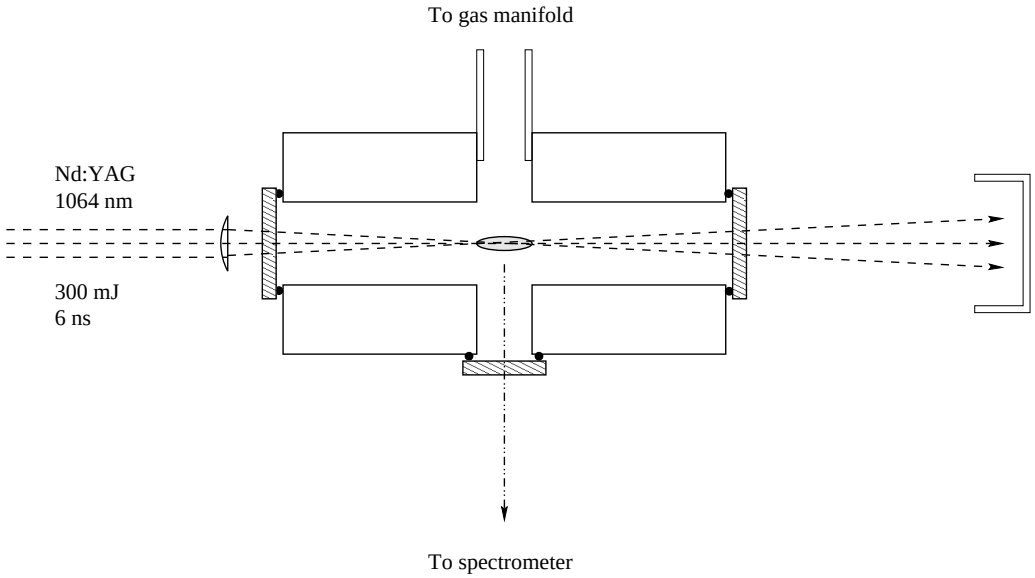

Fig. 1. The infrared (1.064 μm) fundamental of a pulsed Nd:YAG laser is focused into a high pressure cell by a 10 cm focal length plano-convex lens. Typically, an energy of 300 mJ is used for these experiments, and a pulse duration of 6 ns. The plasma, produced between the entrance window and the vacuum focal point, is imaged through a side window onto the entrance slit of a spectrometer or spectrograph. The spectrum is detected with a CCD camera or a fast photodiode.

A related problem of optical damage to the entrance window was encountered which is to be expected when focusing Nd:YAG laser light at the energies used here. The degree of damage can be monitored, but self-focusing within the window does lead to sudden failure once a defect occurs. In this case, the failure can be very hazardous because the contained H_2 is released into air while the excitation laser is operating. The incident laser light reflects off of all optical surfaces and focuses to hot spots outside the cell along the optical path. Breakdown may occur in these spots while the experiment is operating, and thus failure of the entrance window would lead to an explosion when the H_2 ignited. We placed a limit on the incident laser energy for these experiments to avoid damage to the optics.

The cell was evacuated with a mechanical pump and allowed to outgas until a base pressure of 1 μm was reached. The cell was then connected to a supply of ultrapure H_2 (undetectable levels of CO, CO_2, and CH_4 impurities), flushed and filled to the working pressure. The cell remained connected to mechanical gauges for monitoring pressure during the experiments, but it was disconnected from the supply tank. The spectra show only lines of atomic H, or Raman lines of H_2, so we are assured that the filled source was clean and free of impurities. Furthermore, a residual gas analysis of the cell showed only H_2, and the typical vacuum system impurities of H_2O and pumping fluids which were removed in the outgassing and flushing process of filling the cell.

The observations were made of the regions in the plasma closest to the lens, and generally near the optical axis. With allowance for the shift of the focal point, the side window was placed so that the most luminous region could be imaged onto the slit of a spectrometer. The transfer imaging was done with another 10 cm focal length lens, here usually arranged to enlarge the plasma by a factor of 2 at the slit plane, so that an image of the optical axis of the incident laser was perpendicular to the slit. An aperture at the gas cell limited the field of view to ± 3 mm above and below the axis. Regions of interest could be selected by a mask at the spectrometer, or in imaging spectroscopy, extracted from the data. It is worth noting that at typical shock front velocities of 10 km/s, the shock would pass out of the field in about 300 ns. Optical filters were inserted into the path in front of the slit.

Three different spectrometers and four different detectors were used for these studies in an effort to distinguish whether the features we found were artifacts due perhaps to grating anomalies, internal scattered light or non-uniform detector spectral response. The results which we show here are those that were seen consistently with two different spectroscopic instruments, and with charge-coupled-device (CCD) and time-resolved photodiode detection. We describe here those configurations in more detail.

The spectrometer/spectrographs were both 0.25 m focal length aberration-corrected Czerny-Turner designs, using aspheric mirrors to improve off-axis image quality. The two instruments had different grating sets, and slightly different baffling and internal optical arrangements. The data were taken with two different gratings, a 1 200 lines/mm holographic grating optimized for the visible, and a 150 lines/mm ruled grating, blazed for 500 nm. Both gratings were used in the first order. To suppress second order light, Schott glass filters (OG515, OG550 and RG695) were inserted into the optical path as needed. These filters absorb light below a cutoff wavelength (nominally 5 150, 5 500, or 6 950 Å), and transmit above that wavelength. Their transmission in the regions of interest is a uniform monotonic function of wavelength which is corrected by comparison to a standard blackbody source. Unfiltered data could also be used except at the longest wavelengths of interest where Hβ at 4 861 Å could contaminate spectra in the region above 9 600 Å.

Time-resolved detection was done with biased silicon PIN photodiodes having a rise time of 20 ns. The spectral sensitivity of these detectors peaks at wavelengths below Hα, so in the long wavelength line wing the detector response smoothly decreases as wavelength increases. The current from the photodiode was amplified with a Stanford Instruments SR250 integrator, which provided gating and sampling of the plasma emission after the excitation pulse. The sampled analog signal was digitized and stored by the computer system that also controlled the spectrometer. In this mode of data collection, we usually averaged over 100 laser shots at 10 Hz for each spectral point, and used gate delays sufficient to suppress detection of the excitation light, but sample the highly ionized plasma about 50 ns later. The delay was selected to optimize the far line wing spectrum, since at shorter times Hα is broadened into the continuum, while at later times it narrows and the wing weakens.

We also recorded spectra in a time-integrated mode with a CCD detector. Of the CCD's which we tried, the one which performed best was a SITE $1\,024 \times 1\,024$ back-illuminated, Peltier-cooled camera with 24 μm square pixels. Its spectral response extends to 1.1 μm and is smooth, with a broad peak and 90% quantum efficiency centered at 6 600 Å. The smoothness of spectral response is of concern, since the effects we will describe may be mimicked if the spectral response is not uniform.

Both CCD and photodiode spectra were wavelength calibrated using standard line sources (Hg and A), as well as internal calibration from Hα, the incident laser line, and the occasional anti-Stokes Raman line at very high pressure and laser power. The total system response as a function of wavelength was calibrated against a ribbon filament blackbody source at approximately 2 000 K. The exact temperature of the calibration lamp was measured with an optical pyrometer, and the final experimental spectra were corrected for the theoretical blackbody curve at this measured temperature. This process should remove the dependence on wavelength of the optical system and detector from the measured spectra. The additional assurance that the filters, gratings, and detectors used all had monotonic wavelength dependence in the region from the Hα line center at 6 563 Å out to 1 μm should guarantee that the spectra in this region are free of artifacts.

Figure 2 shows the experimental spectrum of the Hα line wing from 5 000 Å to 9 600 Å derived from the time-resolved measurements. The data shown were taken at a source pressure of 10 000 KPa and a delay of 48 ns. The delay time was optimized to yield the most pronounced line wing. The error bars are derived from the signal-to-noise ratio in the original data, and are wavelength-dependent. In addition to the calibration for spectral response, there is a question about background and the correct zero-light level. The time-resolved data always had an uncertain fixed reference bias due to the sampling and digitizing system, and to residual stray light in the spectrometer. In the data shown we have adjusted this so that the signal above 1 μm is zero except close to the laser line. We detect the incident laser line, even at an electronic delay of 48 ns,

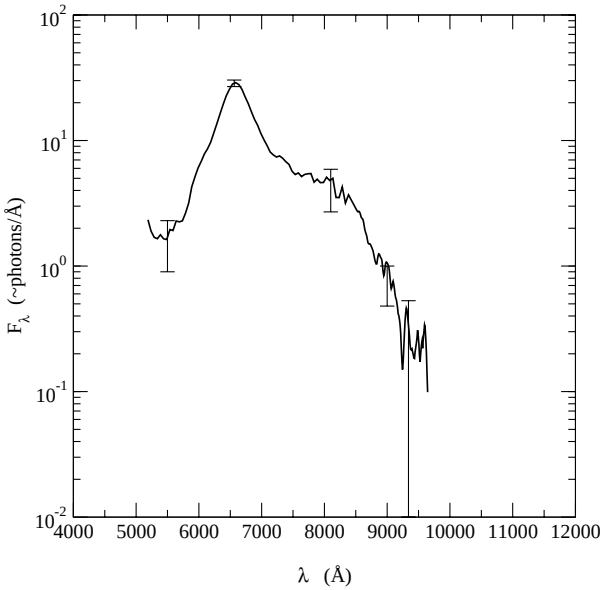

Fig. 2. A spectrum of Balmer α measured for a laser-produced plasma in H_2 48 ns after the laser pulse. The error bars indicate the rms signal-to-noise ratio in the original data.

since the detector response has an exponential decay and the laser scatter (due to filamentation and beam breakup) is extremely intense in these high pressure spectra.

We note the very broad Hα line and the continuum from shorter wavelengths where Hβ (not shown) has been broadened to the degree that it is not distinguishable. We cannot say *a priori* what the neutral, ion, and electron densities are that are responsible for this spectrum. The diagnostics we have on the source are known to be reliable for lower pressures where we can be assured that almost all of the incident laser energy couples to the plasma. At the higher pressures of these experiments, there is considerably more loss of laser energy because of channel formation and because the beam self-focuses, and forms filaments which then defocus and deflect the light. However, we have a guide in that at electron densities well above 10^{19} cm^{-3} Hα should disappear because the series limit advances to include $n = 3$ when Stark broadening dominates [20]. Also, at temperatures much above 10 000 K atomic hydrogen will ionize and deplete the number of neutral atoms that can radiate. Our simulations of the plasma suggest that at this delay time the ion and neutral densities will be comparable in the region contributing to the line emission, and that this density will be of the order of a few percent of the density of atomic H if the H_2 gas were dissociated. This lowered density is because the shock front produced by the laser compresses the ambient gas, but the emission is from behind the front where the hot rarified gas is moving outward. Also, although the filling pressure of 10 000 KPa corresponds to 5×10^{21} ions cm^{-3} if the gas were fully dissociated and ionized, Hα line emission cannot arise from such high density. Our observations are selective in this sense, and record emission from the regions where neutral atoms can exist in the $n = 3$ state.

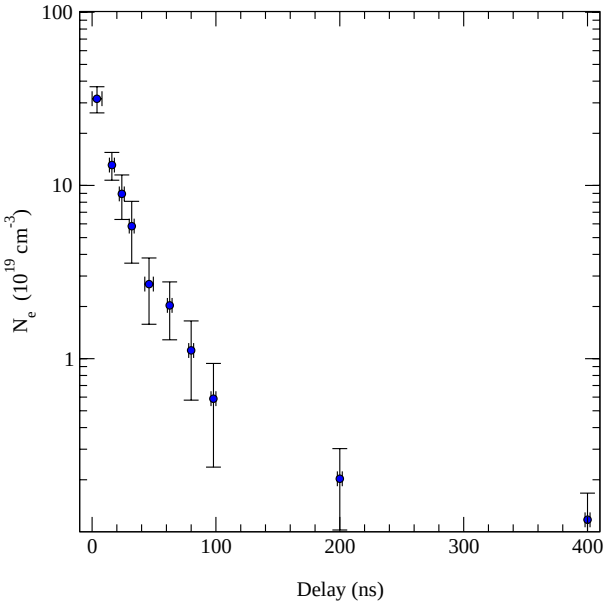

Fig. 3. The plasma electron density as a function of delay after the laser pulse, determined from the full width of the Hα core.

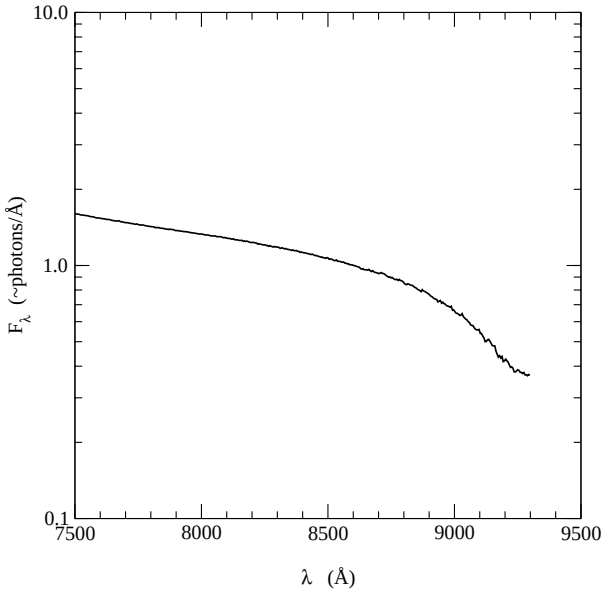

Fig. 4. The Balmer α line wing from a laser-produced plasma, recorded with CCD imaging spectroscopy. The spectrum represents the integration over time of the emitted spectrum.

On this basis, we expect that the optical line emission is from a region that has a ion or electron density a few times 10^{19} cm^{-3}, and a temperature of the order of 10^4 K.

The full width at half maximum intensity of the Hα line core was measured by fitting the line within a few widths of center to a Lorentzian on a quadratic background. These widths may be related to the electron density given a suitable theory of the core that includes broadening by electron collisions. The calculations of the width by Kepple and Griem [21] have been tested experimentally at densities below 10^{19} cm^{-3}, the lower limit of density for which we have line wing data. Figure 3 shows that, based on the line core, the ion density decreases from more than 10^{20} just following the laser pulse, to less than 10^{19} after 100 ns. At the time the measurement of the profile shown in Figure 2 was made, the density derived from the line core width was approximately 3×10^{19} cm^{-3}.

The most striking feature of the spectrum in Figure 2 is that the long-wavelength wing of Hα has a shoulder between 8 000 and 9 000 Å. This behavior is similar to that observed in other spectral lines when photons are emitted while the radiator is in close collision with a perturber. As we will see, the "satellite" seen here may have its origin in the transient quasimolecular states of excited H atoms interacting with protons in the plasma.

Figure 4 is a time-integrated spectrum recorded with a CCD detector, with the same source initial conditions. Without time resolution the averaged line profile for Hα is much narrower, and the spectrum close to the line center is dominated by late emission from atoms in the cooling rarified gas when the ion and electron density is much lower. The far wing, however, is produced primarily when the plasma is hot and ionized, so that time integration still detects the effects of close radiative collisions in the dense plasma that lead to the appearance of satellites. This detection method produces better signal-to-noise ratio than digitizing the gated signal from a single photodiode, although it is also more influenced by light scattered from the intense line center. The profiles in the satellite region shown in Figures 2 and 4 are similar, and the differences may be attributed to the different sources of instrumental scattering in the two types of measurement.

The weight of the experimental evidence from spectra of ionized high density atomic H is that the Hα line region contains structure that has the characteristics expected of features due to atom-ion collisions. In the following section we investigate the theory of this process and compute spectra for comparison with these experiments.

3 Theoretical spectra

3.1 General expression for the spectrum

A unified theory of spectral line broadening has been developed to calculate neutral atom spectra given the interaction and radiative transition moments for relevant states of the radiating atom with other atoms in its environment. Complete details and the derivation of the theory are given by Allard *et al.* [6].

In this approach, the profile is given as the Fourier transform of an autocorrelation function which is written as

$$F_\nu(\Delta\nu) = \mathsf{FT}\left[\exp\left(ng(s)\right)\right] \quad (1)$$

where the Fourier transform is taken such that $F_\nu(\Delta\nu)$ is normalized to unity when integrated over all frequencies, and $\Delta\nu$ is measured relative to the unperturbed line.

For a transition $\alpha = (\mathrm{i}, \mathrm{f})$ from initial state i to final state f, we have

$$g_\alpha(s) = \frac{1}{\sum_{e,e'}{}^{(\alpha)} |d_{ee'}|^2} \times \sum_{e,e'}{}^{(\alpha)} \int_0^{+\infty} 2\pi\rho\,\mathrm{d}\rho \int_{-\infty}^{+\infty} \mathrm{d}x\; \tilde{d}_{ee'}[\,r(0)\,] \times \left[\mathrm{e}^{\frac{\mathrm{i}}{\hbar}\int_0^s \mathrm{d}t\; V_{e'e}[\,R(t)\,]}\; \tilde{d}^*{}_{ee'}[\,R(s)\,] \;-\; \tilde{d}_{ee'}[\,R(0)\,] \right]. \quad (2)$$

The e and e' label the energy surfaces on which the interacting atoms approach the initial and final atomic states of the transition as $R \to \infty$. The asymptotic initial and final state energies are E_i^∞ and E_f^∞, such that $E_e(R) \to E_\mathrm{i}^\infty$ as $R \to \infty$. We then have R-dependent frequencies

$$\nu_{e'e}(R) \equiv (E'_e(R) - E_e(R))/h \quad (3)$$

which become the isolated radiator frequency ν_if when perturbers are far from the radiator. The total line strength of the transition is $\sum_{e,e'} |d_{ee'}|^2$. The radiative dipole transition moment of each component of the line depends on R, and changes during the collision. At time t from the point of closest approach for a rectilinear classical path

$$R(t) = \left[\rho^2 + (x + vt)^2\right]^{1/2}, \quad (4)$$

where ρ is the impact parameter of the perturber trajectory, and x is the position of the perturber along its trajectory. We define $\tilde{d}_{ee'}(R(t))$ as a *modulated* dipole [6]

$$\tilde{d}_{ee'}[R(t)] = d_{ee'}[R(t)]\mathrm{e}^{-\frac{\beta}{2}V_e[r(t)]}\,. \quad (5)$$

The difference potential is

$$V_{e'e}(R) = V_{e'}(R) - V_e(R), \quad (6)$$

where the potential energy for the state is

$$V_e(R) = E_e(R) - E_e^\infty. \quad (7)$$

In the above, we neglect the influence of the potentials $V_e(r)$ and $V_{e'}(r)$ on the perturber trajectories, which remain straight lines. Although we should drop the Boltzmann factor $\mathrm{e}^{-\beta V_e(r)}$ for consistency with our straight trajectory approximation, by keeping it we improve the result in the wings where its effects are significant.

3.2 Balmer α in H–H$^+$ collisions

Our theoretical approach is based on the quantum theory of spectral line shapes of Baranger [22,23] developed in an *adiabatic representation* to include the degeneracy of atomic levels [2,24,25].

An H_2^+ correlation diagram for Balmer α and Lyman β (Tab. 1 in Ref. [4]) gives us the orbitals of the united atom correlated to the $n = 1$, 2, and 3 levels of the separated atoms. Only transitions between states of opposite parity and having $|m - m'| = 0, 1$ are dipole allowed.

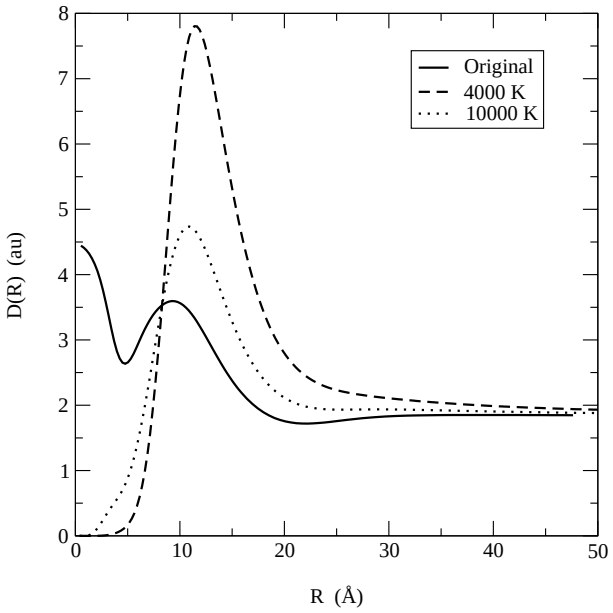

Fig. 5. Variation of the modulated radiative dipole moment for the $3u7g$ transition with temperature.

For the $n = 2$, and $n = 3$ levels there are many energy surfaces which lead to a same asymptotic energy at $R \to \infty$ and, finally, there are 32 molecular transitions which contribute to Balmer α. A tabulation of them is given by Decrette [26].

The complete profile depends on the radiative dipole moment as a function of interatomic separation [6]. A major improvement compared to previous work is that now we take into account the Boltzmann factor in emission. Figure 5 shows large changes in the amplitude of the *modulated* dipole moment in emission with temperature compared to the original dipole transition moments $d_{ee'}(R)$ calculated by Ramaker and Peek [15].

3.3 Balmer α profile perturbed by protons

The evaluation of equations (1, 2) has been done for temperatures and densities which are expected in the laser-plasma source on the basis of the blastwave analysis.

The profile dependence on ion density is shown in Figure 6. Line profile calculations shown here have been done at a temperature of 4 000 K for different densities of protons from 10^{15} to 10^{20} cm^{-3}. These calculations have been done without using the expansion in density which is used only at the lowest density (10^{15} cm^{-3}). Consequently these profiles are valid from the center to the far wing and allow a comparison of the amplitudes of the satellites to the line core.

A region in which the intensity goes through a shoulder or even an increase with increasing separation from the

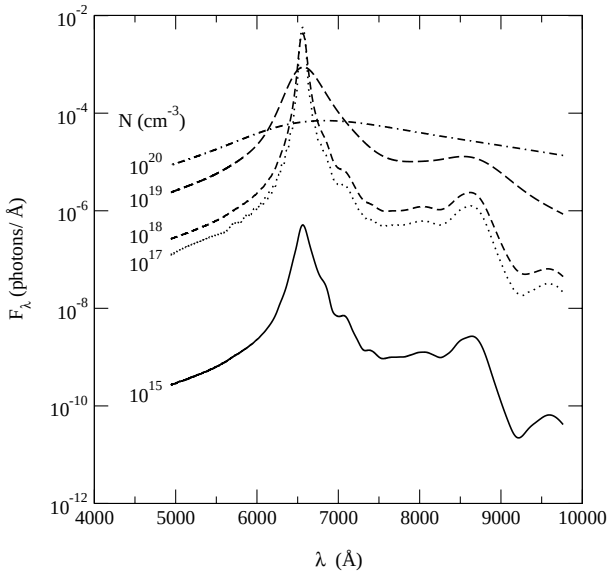

Fig. 6. Comparison of Balmer α profiles with modulated dipole moment at several different densities of H^+ in units of cm^{-3}.

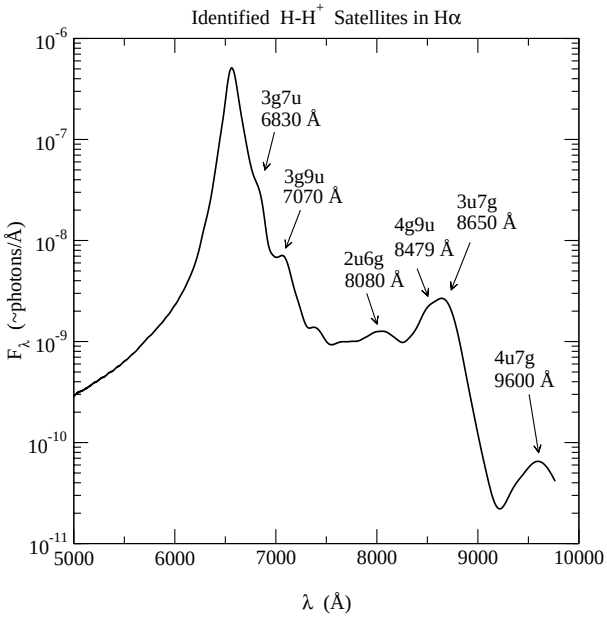

Fig. 7. Identification of the line satellites in Hα total profile broadened by 10^{15} H^+ ions cm^{-3}. The temperature is 4 000 K. The theory includes the variation of the radiative dipole moment with atom-ion separation and the Boltzmann factor for emission.

line center is termed a "satellite" in the line shape literature. Extrema in the difference potential energy surfaces should give rise to satellites in the far wing of Balmer α. Several difference potentials for the allowed transitions of H_2^+ have extrema and are expected to exhibit associated excited atom-proton binary collision satellites.

To allow the best identification of the transitions which give a line satellite we present in Figure 7 the line profile calculation at 10^{15} cm^{-3}. There are two very distinct satellites predicted by the theory, at 8 650 Å, and at 9 600 Å. There are also shoulders on the line core at 6 830 Å and 7 070 Å and shoulders on the 8 650 satellite at 8 080 and 8 479 Å. The other satellites blend into the profile. Table 1 lists the upper and lower state identifications and the wavelength of the predicted satellites.

The satellite at 8 650 Å is a prominent feature and is seen in the laboratory experiments. As Figure 8 shows, the reason for this is that the difference potential energy for this satellite passes through a minimum at a relatively large internuclear distance of 13 Å. As a consequence, the average number of perturbers in the interaction volume is large, leading to a high probability of binary collisions, and making a satellite strong enough to appear distinctly. The intensity of these satellites depends not only on the probability of the collision which produces them, but also on the radiative dipole moment of the transient multiatom system. The probability increases with atomic density, and it may be enhanced by the collision dynamics and the Boltzmann factor for the excited state. The radiative dipole moment changes significantly in close collisions from its asymptotic value for the unperturbed atom as it can be seen in Figure 8, where we have displayed $D(R)$ together with the corresponding $\Delta\omega(R)$ for the transition which should produce the 8 650 Å satellite.

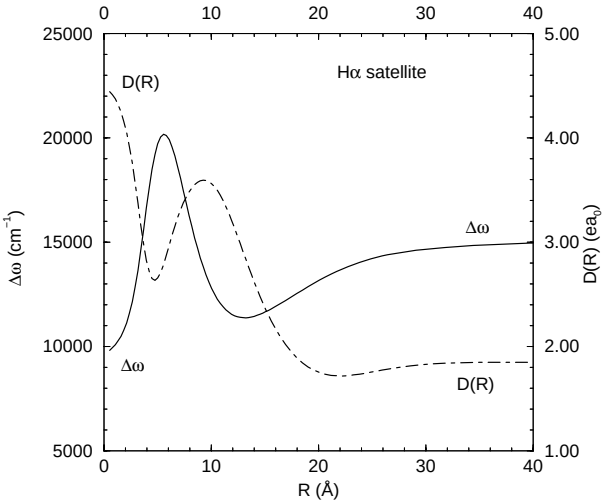

Fig. 8. Radiative transition moment and the $3u7g$ transition difference potential as a function of interatomic distance. The figure shows that large changes in the amplitude of the radiative dipole moment occur when one perturber is near the extremum in the potential difference.

4 Comparison with theoretical line shapes

In Figure 9 we compare a grid of theoretical calculations with the observed spectrum. The best agreement in shape is at a density of about 3×10^{19} cm^{-3}, the same density found from the line core width at the delay time of these measurements. This is the density at which the 8 650 Å satellite begins to disappear into the extreme wing, making the shape very dependent on proton density here.

Table 1. Satellites due to H–H^+ collisions.

NRP*	upper level	lower level	weight	$\lambda_{H_2^+}$ (Å)	$\Delta\omega_{H_2^+}$ (cm^{-1})	R_{pot} (Å)
$3g7u$	$6h\ \sigma_u$	$3d\ \sigma_g$	1	$6\,869^a$	-681^a	23.0
				$6\,830^b$		
$3u7g$	$5g\ \sigma_g$	$4f\ \sigma_u$	1	$8\,756^a$	$-3\,819^a$	13.2
				$8\,650^b$		
$4u7g$	$5g\ \sigma_g$	$2p\ \pi_u$	2	$9\,725^a$	$-4\,956^a$	12.7
				$9\,600^b$		
$4g9u$	$4f\ \pi_u$	$3d\ \pi_g$	1	$8\,624^a$	$-3\,644^a$	9.3
				$8\,479^b$		
$2u6g$	$4d\ \sigma_g$	$3p\ \sigma_u$	1	$8\,312^a$	$-3\,208^a$	6.3
				$8\,080^b$		

* Notation of Ramaker and Peek [15]. ^{a} Predicted from the isolated potential extremum. ^{b} Apparent in the total profile.

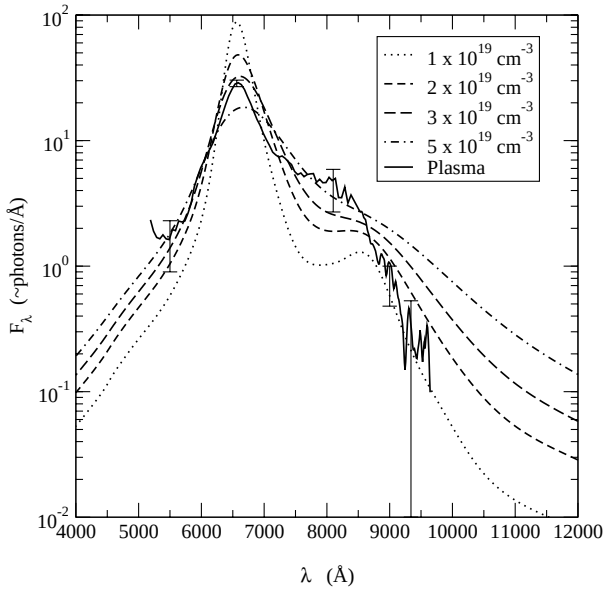

Fig. 9. A comparison of Balmer α as seen in these experiments with profiles calculated with an R-dependent electronic transition dipole moment. The theoretical profiles have been scaled in strength for comparison with the experiment.

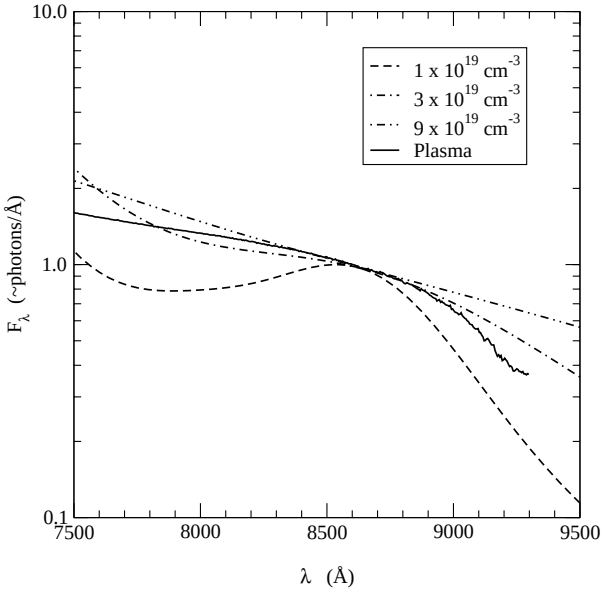

Fig. 10. A comparison of the Balmer α as seen in the time integrated experimental data with theoretical profiles at different ion densities.

The shape should also depend critically on broadening by electrons and neutrals, effects not yet included in this calculation. For a complete comparison, it would be therefore necessary to take into proper account the total contribution of both the protons and electrons so far in the line wing, as well as the contributions of neutral atoms. A complete set of molecular data for the neutral atom-atom collisions in the $n = 3$ states are not yet available, and consequently we cannot yet compute the complete profile including all these effects. Nevertheless preliminary line profile calculations using *ab initio* calculations of Spielfiedel [27] of molecular potentials and electronic transition moments for excited states of the H_2 molecule were done. It has been shown [28] that distinct neutral collision satellites on Balmer α satellites are expected in the visible range as well in the near infrared. The presence of these effects together with the ion-collision satellites could account for the differences we see between the experiments and the theory that includes only ion collisions.

In Figure 10 we again compare the theoretical profiles in the region of the 8 650 Å satellite due to H–H^+ interaction with another experimental profile. The experimental data shown in this figure have higher signal-to-noise ratio, but are influenced by the integration in time over the emission. The comparison is useful only in the satellite region, since that emission will only occur during a narrowly defined period as the plasma expands. It is not possible to compare the satellite recorded in this way with the line center, however, since the line is emitted strongly over a longer time, and is much narrower at later times than when denser plasma emits the satellite. In spite of

this shortcoming, the spectrum reveals a satellite that is a very distinct feature in the Balmer α wing. Its position in the theoretical profile is in approximate agreement with the observations.

5 Conclusions

The unified theory of spectral line broadening applied to the Balmer α line of atomic hydrogen predicts structure in the Balmer α line wing due to radiation that is emitted during atom-ion collisions. The evaluation of the theory reported here takes into account the 32 states of the H_2^+ quasi-molecule that contribute to Balmer α in a hydrogen plasma, and includes the effects resulting from the dependence on atom-ion separation of the radiative dipole transition moment. While six satellites are identified in the theoretical wing on the long-wavelength side of the unperturbed line center, the single strongest feature is a satellite at 8 650 Å. At ion densities from 10^{19} cm^{-3} to 10^{20} cm^{-3}, the 8 650 Å satellite increases in significance as the line broadens until the satellite is lost in a very broadened and shifted profile for densities greater than 10^{20} cm^{-3}.

Laboratory observations of a laser-produced hydrogen plasma confirm that the 8 650 Å satellite exists in the Balmer α red wing. The experiments demonstrate the significance of broadening by electrons, and probably also by neutrals, in the far wing spectrum, but when the degree of ionization is high the unified theory used here accounts well for the observed structure.

We should be able in the near future to do calculations of the total profile of the atomic hydrogen Balmer α spectral line perturbed by simultaneous collisions with neutral hydrogen atoms and protons. However, the problem of an accurate accounting for electron broadening as well as ion and neutral broadening with a consistent unified theory so far in the wing remains.

The work at the University of Louisville was supported by grants from the U.S. Department of Energy, Office of Science, Division of Chemical Sciences.

References

1. J. Kielkopf, Phys. Rev. E **52**, 2013 (1995).
2. N. Allard, D. Koester, N. Feautrier, A. Spielfiedel, Astron. Astrophys. **200**, 58 (1994).
3. J. Kielkopf, N. Allard, Phys. Rev. A **58**, 4416 (1998).
4. N. Allard, J. Kielkopf, N. Feautrier, Astron. Astrophys. **330**, 782 (1998).
5. N. Allard *et al.*, Astron. Astrophys. **335**, 1124 (1998).
6. N. Allard, A. Royer, J. Kielkopf, N. Feautrier, Phys. Rev. A **60**, 1021 (1999).
7. N. Allard, J. Kielkopf, I. Drira, P. Schmelcher, Eur. Phys. J. D **12**, 263 (2000).
8. J. Kielkopf, N. Allard, Astrophys. J. **450**, L75 (1995).
9. P. Bergeron *et al.*, Astrophys. J. **449**, 258 (1995).
10. D. Koester, G. Vauclair, in *White Dwarfs*, edited by J. Isern, Z. Hernanz, E. Garcia-Berro (Kluwer, Dordrecht, 1997), p. 429.
11. D. Koester *et al.*, Astrophys. J. **463**, L93 (1996).
12. D. Koester *et al.*, Astron. Astrophys. **336**, 276 (1998).
13. H. Holweger, D. Koester, N.F. Allard, Astron. Astrophys. **290**, L21 (1994).
14. M.M. Madsen, J. Peek, At. Data **2**, 171 (1971).
15. D. Ramaker, J. Peek, J. Phys. B **5**, 2175 (1972).
16. H. Griem, *Principles of Plasma Spectroscopy* (Cambridge University Press, Cambridge, 1997).
17. J. Kielkopf, Phys. Rev. E **63**, 016411 (2001).
18. W. Wiese, D. Kelleher, D.R. Paquette, Phys. Rev. A **6**, 1132 (1972).
19. S. Boddeker *et al.*, Phys. Rev. E **47**, 2785 (1993).
20. H. Griem, *Plasma Spectroscopy* (McGraw-Hill, New York, 1964), 124.
21. P. Kepple, H.R. Griem, Phys. Rev. **173**, 317 (1980).
22. M. Baranger, Phys. Rev. **111**, 481 (1958).
23. M. Baranger, Phys. Rev. **112**, 855 (1958).
24. A. Royer, Can. J. Phys. **52**, 1816 (1974).
25. A. Royer, Phys. Rev. A **22**, 1625 (1980).
26. A. Decrette (unpublished).
27. A. Spielfiedel (unpublished).
28. M. Leseignoux *et al.*, in *Proceedings of SF2A 2001*, Lyon, May 28–June 1st (EDP Sciences, 2001).